






RESEARCH ARTICLE | NOVEMBER 09 2023


Effects of pre-chamber flow-field on combustion stability in a spark-ignition engine using large-eddy simulations

R. Novella ; J. M. Pastor ; J. Gomez-Soriano  ; I. Barbery 




Physics of Fluids 35, 115116 (2023)

<https://doi.org/10.1063/5.0169655>



Physics of Fluids
Special Topic:
Flow and Climate
Guest Editors: Khaled Ghannam and Mostafa Momen
[Submit Today!](#)



Effects of pre-chamber flow-field on combustion stability in a spark-ignition engine using large-eddy simulations

Cite as: Phys. Fluids **35**, 115116 (2023); doi: [10.1063/5.0169655](https://doi.org/10.1063/5.0169655)

Submitted: 27 July 2023 · Accepted: 20 October 2023 ·

Published Online: 9 November 2023



View Online



Export Citation



CrossMark

R. Novella,  J. M. Pastor,  J. Gomez-Soriano,^{a)}  and I. Barbery 

AFFILIATIONS

CMT – Clean Mobility & Thermofluids, Universitat Politècnica de València, Camino de Vera, Valencia 46022, Spain

^{a)} Author to whom correspondence should be addressed: jogoso1@mot.upv.es. Tel.: +34 96 387 98 13. Fax: +34 96 387 76 59

ABSTRACT

Significant efforts are under way to develop innovative ignition systems for spark-ignition engines used in transportation. Within this context, passive pre-chamber technology has emerged as a promising alternative for passenger cars. However, several uncertainties remain regarding the operation of this concept at low engine loads and speeds, as well as the impact of specific design features on combustion stability. Previous investigations have indicated that the tangential angle of the pre-chamber holes can play a vital role in stabilizing the combustion process. Nonetheless, the underlying thermo-physical phenomena responsible for these results have not yet been thoroughly studied. To address these knowledge gaps, this paper presents a numerical study using a computational fluid dynamics model that has been validated with experimental results. An alternative modeling methodology was developed to conduct multi-cycle large-eddy simulations and investigate two different pre-chamber configurations, one with tangential holes and the other with radial holes. The results revealed an intriguing correlation between the combustion stability and the spatial distribution of the flame inside the pre-chamber. The cycle-to-cycle dispersion of pre-chamber flow variables was significantly higher when using radial holes compared to tangential holes, potentially explaining the unstable behavior of the former design. Additionally, the undesirable flow-field of the radial-hole pre-chamber caused the flame to evolve asymmetrically, resulting in substantial variations in the ejected jets. This asymmetry can significantly affect the morphology of the main chamber ignition in each cycle.

Published under an exclusive license by AIP Publishing. <https://doi.org/10.1063/5.0169655>

I. INTRODUCTION

Over the past years, the irruption of electric vehicles in the automotive market as clean and affordable transportation options has increased the demand for engine manufacturers to develop alternative solutions for reducing the environmental impact of current internal combustion engines (ICEs).¹ Projections made by international organizations toward the upcoming decades show that by 2050 most means of energy production are still expected to be fossil fuel dependent;² therefore, the society may be facing a considerable hike in the generation of greenhouse gases only attributed to this increasing energy demand.

Considering that the transportation sector accounts for over 25% of the carbon dioxide (CO₂) emissions in the European Union^{3,4} and that these emissions are mainly produced in road transportation by heavy-duty and light-duty or passenger car vehicles,⁵ there is an urgent need to improve the propulsive systems of these vehicles to reduce their carbon footprint. In this context, spark ignition (SI) engines have

been leading the automotive market over the last couple of decades, with approximately 67% of the total vehicles sold in the European Union in 2022 integrating this type of engines.⁶ Nevertheless, SI engines have important limitations in terms of thermal efficiency compared to equivalent compression ignition (CI) engines, mainly due to knocking issues, an abnormal combustion phenomenon that compromises the mechanical integrity of the cylinder and prevents the use of high compression ratios.^{7,8}

One of the most promising solutions for increasing the efficiency and reducing the emissions of future SI engines is the integration of enhanced combustion strategies and advanced ignition concepts.^{9,10} Among the different ignition systems that are available, the pre-chamber ignition concept has been gaining a lot of interest in recent years.^{11–13} This technology has been evolving since the 1920s as a strategy to increase the burn rates and prevent the appearance of engine knock.¹⁴ Currently, the pre-chamber system has been implemented in applications such as high-power stationary powerplants, marine

engines, and Formula 1;^{15–17} however, its implementation in SI engines for passenger car applications is still under development.

This ignition strategy places the standard spark plug inside a confined volume called a “pre-chamber,” which is connected to the combustion chamber (main chamber) through one or several holes manufactured at the bottom of the pre-chamber. As combustion progresses within the pre-chamber, the pressure in this region rises and a series of hot gaseous jets are ejected through the holes into the main chamber, igniting the charge with a larger flame surface at multiple locations.¹⁸ The jets distribute burned products as they sweep the main chamber volume, generating uniform and dispersed ignition,¹⁹ accelerating the burn rates, mitigating knocking combustion,²⁰ and enabling to burn lean mixtures.²¹

Most real-world pre-chamber applications implement this technology through an active approach that requires the assembly of a dedicated injection system inside the pre-chamber to control its equivalence ratio independently from that available in the main chamber.^{22,23} However, the additional expenses of duplicating the injection system compromises its integration in SI engines for passenger car applications, in which costs are critical and can determine the success or failure of this ignition strategy. Therefore, a different alternative is to use a passive system, where the pre-chamber fills only due to the piston compression, facilitating its integration into the current versions of many commercial engines, since the pre-chamber can be mounted directly into the conventional spark plug housing.^{24,25}

Nevertheless, since the passive approach loses one degree of freedom by not being able to control the air-to-fuel equivalence ratio inside the pre-chamber, the thermo-fluid-dynamic processes inside this region become of critical importance. Thus, it is necessary to design the pre-chamber geometry in a way that allows a suitable scavenge and favorable flow conditions to be generated for optimizing the combustion process. Furthermore, despite many research works have been devoted to analyze the effects of basic pre-chamber geometry features such as hole diameter and volume,^{26,27} there is still an important knowledge gap regarding the effects of more advanced geometrical parameters such as the internal pre-chamber design and the configuration of the holes (orientation, disposition, etc.).

One of the major hurdles that has hindered the integration of the passive pre-chamber system into commercial passenger car engines is related to the characteristic small size of the pre-chamber, which limits the correct operation of this concept in certain regions of the engine map. Previous studies performed by Benajes *et al.*^{28,29} revealed that using the passive pre-chamber allows to gain 3% points of efficiency compared to the standard spark plug when operating under knock limited conditions (i.e., high engine load/speed conditions). However, several investigations have shown important limitations under conditions where the combustion process is compromised due to the low amount of fuel (part-loads) or the worsened thermo-fluid-dynamic properties of the mixture (low engine speed).³⁰ A recurrent issue found in the literature is the inability to delay the combustion process toward the expansion stroke when operating in idle or cold-start conditions,³¹ where a sharp increase in the cycle-to-cycle variability (CCV) is observed as the spark timing is pushed toward the top dead center (TDC), destabilizing the engine operation and compromising the efficiency levels.³² Moreover, a previous research by Novella *et al.*³³ also showed that using a pre-chamber with completely radial holes generates very high levels of CCV when operating at low load/speed

conditions, which is an important design limitation that is yet to be analyzed in depth.

To study complex phenomena such as combustion and CCV in SI engines, computational fluid dynamics (CFD) models using large-eddy simulations (LES) have proven to be an accurate approach.^{34–36} Therefore, this research work focuses on developing an innovative multi-cycle LES modeling methodology for studying the CCV of pre-chambers with tangential and radial holes operating at low load/speed conditions in a light-duty SI engine. The methodology aims to overcome the usual limitations regarding computational resources for performing LES. This novel investigation will improve the knowledge of the passive pre-chamber ignition system, particularly the operation in one of the most critical points of the engine map and the effects of hole orientation over the combustion stability of a given pre-chamber design, providing relevant contributions to the current state-of-the-art.

II. RESEARCH TOOLS AND METHODOLOGY

To address the knowledge gaps of the passive pre-chamber concept that were highlighted in Sec. I, a combination of experimental and numerical tools was used. This research starts by presenting the issues found in an experimental campaign carried out by the authors, related to the performance of a particular pre-chamber design at low load/speed conditions. Thereafter, a CFD model, validated with the experimental results, is used to explore the root causes of these issues following a clever methodology for performing multi-cycle combustion simulations.

A. Experimental framework

The experimental environment is made up of a single-cylinder 4-stroke turbocharged SI engine, representative of those currently found in passenger cars, and a fully equipped test bench designed to operate this type of engines. The most relevant features of this powertrain include the combination of a low cylinder displacement (404 cm³) and a high compression ratio (13.4:1), a port fuel injection (PFI) system to ensure a well-mixed air/fuel blend to enter the cylinder, two sets of intake/exhaust valves with double-overhead camshafts, and a small housing on the cylinder head for an M12 spark plug with the passive pre-chamber integrated. Table I shows a summary of these features.

The test cell incorporated several measurement devices and instrumentation for monitoring the most relevant parameters during the engine operation, including piezoelectric and piezoresistive sensors to obtain the instantaneous pressure signals in the cylinder and the intake/exhaust ports, a liquid fuel supply system for a RON95 (95 research octane number) calibrated gasoline that included an AVL

TABLE I. Main specifications of the engine.

Engine	4-stroke SI
Number of cylinders (–)	1
Displacement (cm ³)	404
Bore–Stroke (mm)	80.0–80.5
Compression ratio (geometric) (–)	13.4:1
Valvetrain (–)	DOHC
Number of valves/cylinder (–)	2 intake and 2 exhaust
Fuel injection system (–)	PFI ($p_{\max} = 6$ bar)

TABLE II. Main properties of the fuel.

Type	Gasoline RON95
H/C ratio (mol/mol)	1.761
Stoichiometric A/F (-)	14.374
Lower heating value (LHV) (MJ/kg)	42.493
Density (15 °C) (kg/m ³)	843.8
Reduced formula (C _x H _y O _z)	7.594 (x) – 13.376 (y) – 0.0 (z)

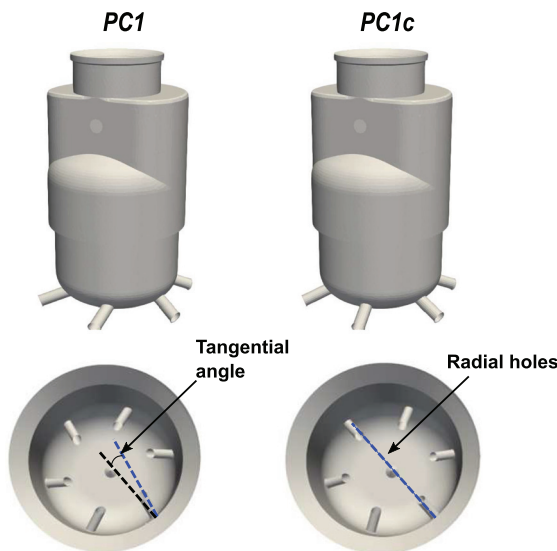


FIG. 1. Schematic of the hole layout for PC1 and PC1c.

733S fuel mass meter and an AVL 753 conditioning system to regulate the fuel temperature, and a HORIBA MEXA 7100 DEGR exhaust analyzer for monitoring the air-to-fuel ratio inside the main chamber. The main properties of the fuel are presented in Table II, while the full details of the experimental facilities can be found in several investigations published in the literature.^{28,32}

Figure 1 shows a sketch of the tested pre-chambers with their main geometrical features summarized in Table III. Moreover, a combination of low engine load and speed, representative of idle or cold-start conditions, was selected as the operating point for the experimental activities with the details presented in Table IV. As stated in the introduction, several investigations have reported issues when operating with passive pre-chambers under these conditions, highlighting the

TABLE III. Geometrical parameters of the tested pre-chambers.

ID	PC1	PC1c
Volume (mm ³)	600	600
Number of holes	6	6
Hole diameter (mm)	0.7	0.7
Tangential angle (°)	12.5	0

TABLE IV. Operating conditions used in the experiments.

Parameter	Value
Engine speed (rpm)	1350
IMEP (bar)	2.8
Injected fuel (mg/cc)	8.4
λ (-)	1
EGR rate (%)	0
MBT spark timing (CAD BTDC)	20
Intake pressure (bar)	0.39
Exhaust pressure (bar)	1.01
Coolant and oil temperature (K)	300

importance of analyzing the performance of different pre-chamber designs in this operating point. In particular, the purpose of this campaign was to study the effects of using a tangential angle in the layout of the holes (PC1) against using completely radial holes (PC1c).

A spark timing sweep was performed for each pre-chamber design, and the results in terms of indicated efficiency and combustion stability are shown in Fig. 2. These trends were also observed during a previous research carried out by the authors³³ for an engine operating with compressed natural gas (CNG). As it can be seen in Fig. 2, PC1 is able to keep a suitable combustion stability with COV IMEP levels below 3% for a wide range of spark timings, until a sudden spike after -10 CAD (referenced to TDC). On the other hand, PC1c is not achievable a stable combustion regardless of the spark timing. This raises an interesting question: What effects does the swirl motion induced by the tangential holes have on combustion stability? Thus, to address this question, a CFD model of the engine was used.

B. CFD model setup

The CFD model was implemented in the commercial code CONVERGE,³⁷ a CFD software based on the finite volume method and widely adopted in the ICE community due to its capacity to simulate moving boundaries and the integrated adaptive mesh refinement (AMR) tool, that allows the computational mesh to be scaled at runtime to improve the resolution of relevant physical and thermodynamic properties of the flow. The full details and configuration of the model can be found in previous investigations performed by the authors.^{30,38} In this section, only the most relevant model settings and modifications made for this paper will be described.

The mesh discretization was done by the cut-cell Cartesian method available in the CFD code with careful refinements applied to the different regions and boundaries of the domain. Particularly, the pre-chamber cells were reduced down to 0.0625 mm at critical regions like the spark plug gap and the holes, while the AMR algorithm also scaled the mesh down to 0.0625 mm based on the velocity and temperature sub-grid scales of 1 m/s and 2.5 K, respectively, to improve the resolution of the flame and the accelerated flow coming from the holes. A summary of the mesh details and strategies is presented in Table V.

To determine which turbulence model should be used in a CFD simulation, it is critical to establish the application of the specific case study, as well as the demands that must be covered by the numerical model. For example, although RANS models^{39,40} are perfectly suitable

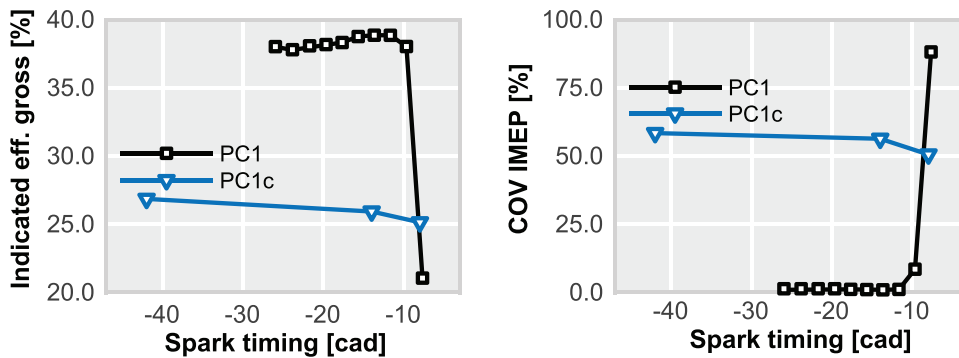


FIG. 2. Experimental results for PC1 and PC1c at low engine load/speed conditions.

TABLE V. Mesh configuration.

Computational region	Cell size (mm)
Intake port	2
Exhaust port	2
Cylinder	0.5
Cylinder walls/piston/valves	0.25
Pre-chamber	0.125
Pre-chamber walls and holes	0.0625
Spark plug gap	0.0625
AMR sub-grid criteria	Minimum cell size (mm)
Temperature: 2.5 K	0.0625
Velocity: 1 m/s	0.0625

for characterizing the global behavior of the flow-dynamics and combustion process in SI engines through single-cycle simulations, the underlying hypothesis of these models does not allow them to account for multi-cycle combustion instabilities due to large turbulent scales.⁴¹ Alternatively, LES models, due to their capacity to resolve these large-scale eddies, are better suited for analyzing the flow-field variations in multiple engine cycles and their impact over the combustion process.⁴² Thus, in the context of this investigation, a dynamic structure sub-grid LES approach has been considered for modeling the sub-grid stress tensor as a function of the sub-grid turbulent kinetic energy (TKE).⁴³

A two-zone flamelet-based model was used to simulate the combustion process. The extended coherent flamelet model (ECFM)^{44,45} employs the flame surface density (Σ) as a means to track the flame front's position, replacing the need for detailed chemistry calculations and thereby reducing the computational time. This model was originally derived and implemented based on a unity Lewis number assumption. The transport of Σ is shown in Eq. (1). Furthermore, the ECFM accounts for various phenomena including the flame stretching due to turbulence (P_1), thermal expansion and curvature of the flame (P_2), and flame surface production due to mean flow dilation (P_3).^{46,47} By using the modeled flame front, the computational domain is divided into burned and unburned regions, employing large-scale species stratification. The progress variable of the combustion model is calculated as a mass fraction of species in the unburned and burned regions of the domain; thus, the ECFM is able to capture up to some

extent the impact of thermal diffusion on the transport of species in the presence of high temperature gradients⁴⁸

$$\frac{\partial \Sigma}{\partial t} + \frac{\partial u_i \Sigma}{\partial x_i} = \frac{\partial}{\partial x_i} \left(\frac{\mu}{S_c} \frac{\partial (\Sigma / \bar{\rho})}{\partial x_i} \right) + (P_1 + P_2 + P_3) \Sigma - D + P_k. \quad (1)$$

Additionally, the ECFM incorporates an integrated imposed stretch spark ignition model (ISSIM) that uses a simplified electrical circuit of the inductive-coil system to simulate the discharge of the spark divided in three phases: The breakdown and arc phases, which are modeled by considering an instantaneous deposition of energy in the gas with the approach proposed by Duclos and Colin,⁴⁹ and the glow phase, which is accounted for by solving the ordinary differential equation of the electrical circuit.⁵⁰ The ignition model considers a user-specified energy input (70 mJ in the case of this research) deposited into a sphere with the radius calculated based on the geometrical inputs provided for the spark plug (distance between electrodes and electrode diameter). This energy input is converted into a reference flame surface density to start the flame propagation through the transport equation for Σ . Thus, the initial flame kernel is considered to be a sphere. However, the ISSIM also includes a tunable constant to account for the initial wrinkling of the flame kernel, which directly increases or reduces the reference flame surface density.

To account for the thermo-chemical properties of the flame, such as flame thickness, laminar flame speed, and auto-ignition delay, the ECFM model uses 4D data tables. For this purpose, 0D well-stirred reactor simulations for ignition delay and 1D laminar flame speed calculations were performed, considering different ranges of pressure, temperature, mixture composition (EGR), and air/fuel equivalence ratio. The detailed methodology for these calculations can be found in a previous study.¹⁸ In Fig. 3, the presented results illustrate the laminar flame speed and auto-ignition delay under high pressures, closely resembling engine-like conditions. Multiple reaction mechanisms for primary reference fuels (PRF)^{51–55} were compared against experimental data at the same conditions.^{56,57} Ultimately, the mechanism proposed by Liu *et al.*⁵¹ was chosen to generate the data tables, as it demonstrated the most accurate predictions.

C. Validation of the CFD model (single-cycle)

Validating the numerical results against experimental data is critical for assuring a suitable calibration of the combustion model to extract meaningful conclusions from the performed simulations. Thus, the maximum brake torque (MBT) conditions of the spark timing

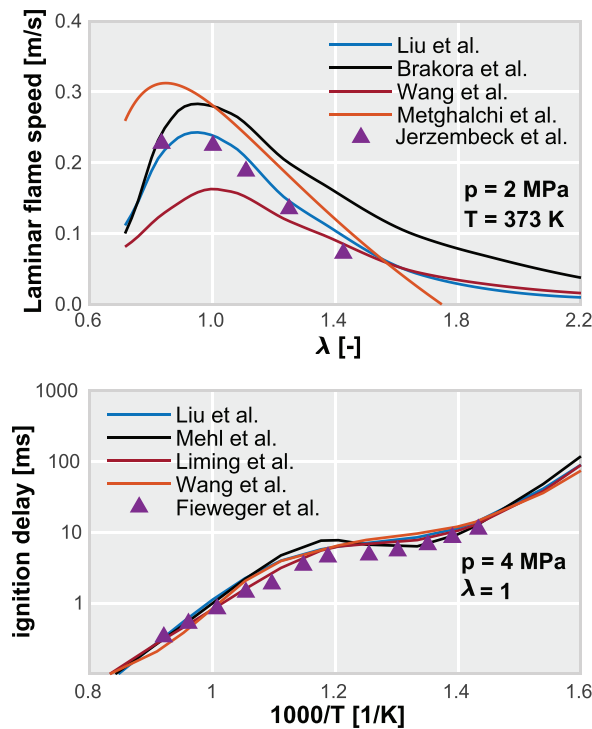


FIG. 3. Auto-ignition delay and laminar flame speed calculations for different chemical kinetics mechanisms at engine-like conditions.

sweep performed for PCI at the operating point presented in Table IV were considered for the model validation. In this case, only one complete engine cycle was simulated and contrasted against the experimental results due to computational restrictions.

The simulation was configured and initialized with the corresponding experimental data (intake/exhaust temperatures, intake/exhaust pressures, injected fuel mass, spark timing, etc.). The lumped model proposed by Torregrosa *et al.*⁵⁸ was used to estimate the wall temperatures for the piston, liner, and cylinder head, from the experimental data in the tested conditions. It is important to point out that a pre-chamber pressure transducer was not available for this research, and thus, the comparison is made with the in-cylinder pressure signal. Results of this comparison are shown in Fig. 4, where the experimental pressure data are averaged over 250 measured cycles and the heat release rate (HRR) is estimated from the pressure signal using an internally developed 0D combustion diagnosis software.^{59–61} It is observed that the simulated pressure trace matches very accurately the experimental signal during the compression and combustion phases, showing a good prediction of the peak cylinder pressure and providing a solid foundation for the analysis to be performed.

Now, if phenomena related to combustion stability and cycle-to-cycle variability are to be analyzed, one step further must be taken and multi-cycle combustion simulations must be performed. Several research works have shown the potential of using a LES formulation in combination with the ECFM combustion model to predict the sources of CCV in SI engines such as the work from Truffin *et al.*⁶² However, the main problem of doing simulations with LES models is the computational cost. These models require very fine meshes, which generate

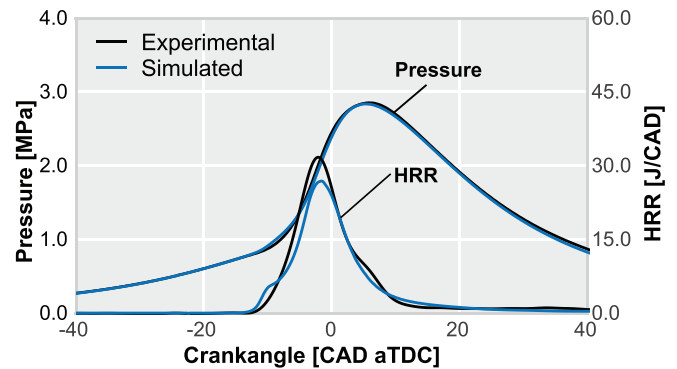


FIG. 4. CFD model validation for low load/speed conditions.

millions of cells in the computational domain, causing the associated computational time to increase significantly, even more so if there is an adaptive refinement algorithm applied to the mesh during the combustion process. For this reason, multi-cycle simulations using the complete engine geometry were unfortunately out of reach with the available computational resources for this investigation.

Therefore, an innovative solution was formulated to overcome the aforementioned limitations. Studies from the literature^{63,64} have shown that early signs of cyclic variability can be observed by analyzing the flow near the spark plug region (in this case inside the pre-chamber) and the initial stages of the combustion process. Thus, there could be important correlations between the flame development during the pre-chamber combustion and the CCV observed in the experiments. From this hypothesis, the multi-cycle simulations can be performed by only considering the combustion in the pre-chamber region. This way, the computational domain is considerably reduced, and a small enough mesh can be used to solve a meaningful amount of the energy spectrum while maintaining reasonable computational times.

D. Multi-cycle LES methodology for pre-chamber combustion simulations

This section describes the methodology that was developed to perform the CCV studies of PCI and PC1c, attributing the cyclic dispersion to changes in the pre-chamber flow conditions and combustion process. This is an alternative approach for performing LES when computational resources are limited.

Figure 5 shows the reduced computational domain, where the pre-chamber has been separated from the complete engine geometry and closed by inflow boundaries placed at the inlet of the holes. In this approach, the simulations are actually performed on a realization-to-realization basis with each realization meaning to represent one combustion cycle. The calculations were divided into non-reacting and reacting cases that will be described below.

The non-reacting case consisted in a single continuous simulation, initialized at the IVC with the same mixture stratification and thermodynamic conditions coming from the open-cycle simulation of the complete engine geometry. The main chamber pressure and temperature profiles of the complete engine simulation were imposed as inflow boundary conditions to artificially replicate the piston dynamics for the pre-chamber filling/empting. These profiles are shown in

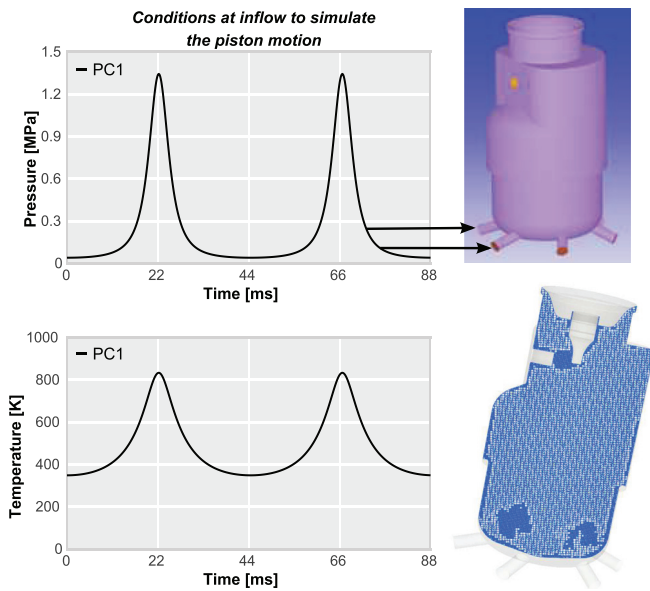


FIG. 5. Computational domain and inflow conditions for the multi-cycle LES.

Fig. 5, perpetually reproduced for each cycle. The flow entering the pre-chamber was considered to have the same mixture composition of the main chamber at IVC (also taken from the complete engine simulation). Furthermore, ten cycles were calculated for both PC1 and PC1c with five instantaneous solutions generated near the TDC of each simulated cycle, corresponding to the crankangles of -25 CAD, -20 CAD, -15 CAD, -10 CAD, and -5 CAD.

Thereafter, the instantaneous flow-fields and mixture distributions were directly mapped from the non-reactive to the reactive simulations, considering equivalent meshes at the moment of ignition. This way, each

TABLE VI. Computational time for one complete cycle using the whole engine geometry and only the pre-chamber.

	Maximum number of cells	Simulation time @64 processors
Whole engine	15 839 562	27 days
Only pre-chamber	2 593 327	2 days

combustion simulation is initialized and develops within a characteristic flow-field with different stratification of species and thermodynamic properties. Figure 6 shows the distribution of residual gases and temperature inside the pre-chamber at the start of multiple combustion cycles.

The combustion model settings were kept equal to the validated full-engine simulation. Moreover, five ignition timings were calculated for each of the ten cycles with both pre-chambers, totaling one hundred simulations, with the reference spark timing being -20 CAD (experimental MBT spark timing for PC1). This approach allowed to study the sensitivity of each pre-chamber to both advanced and delayed spark timings in terms of CCV, to compare these results with the experimental trends found for both designs and search for possible correlations that could explain these trends.

Although the approach adopted in this paper might not be the most accurate strategy as it does not account for thermodynamic and thermo-chemical stratification effects coming from the combustion process in the main chamber, it is an interesting alternative for performing LES with low computational resources. Table VI shows the benefits of the developed methodology in terms of computational cost, which is even more critical when performing studies for practical use-cases where a large amount of simulations are required (such as comparing multiple pre-chamber designs). In addition, meaningful correlations have been found in this investigation that potentially explain the behavior of the studied pre-chambers during the experimental campaign, further supporting the validity of the adopted methodology.

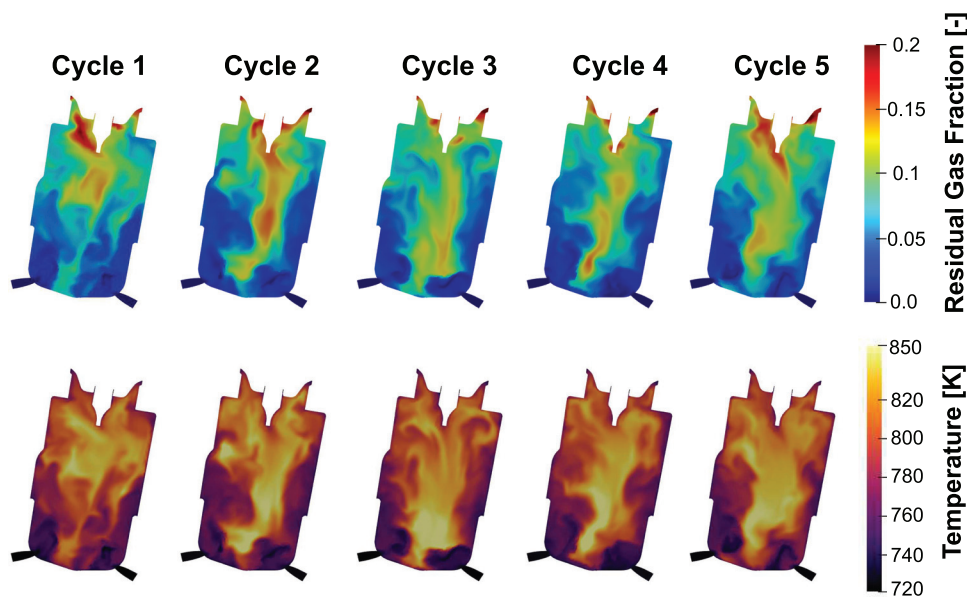


FIG. 6. Distribution of residual gases and temperature inside PC1 at the start of multiple combustion cycles.

III. RESULTS AND DISCUSSION

Before diving into the results, several studies from the literature have shown strong correlations between the cycle-to-cycle variations of SI engines and the initial flow conditions in the proximities of the spark plug.^{63–65} Therefore, the first part of the analysis will focus on characterizing the distribution of the flow variables in the whole pre-chamber and their deviations between cycles, paying special attention to the surroundings of the electrodes.

A. Flow-field analysis of the pre-chamber

To begin, Fig. 7 shows the modeled turbulent kinetic energy field for five consecutive cycles of PC1 (top rows) and PC1c (bottom rows). The snapshots are taken from the non-reacting simulations at an advanced crankangle (−40 CAD) and at the reference spark timing (−20 CAD). The right-side columns show the spatially averaged TKE field for all cycles and the standard deviation (SD) of the TKE in the

full length of the pre-chamber. In this figure, it can be appreciated how the general behavior of the flow-field is very different for both designs. In the case of PC1, the swirling motion induced by the tangential angle of the holes generates high TKE values at the bottom, which quickly dissipates as the flow goes in an upwards spiral along the pre-chamber walls. This pattern appears to be quite uniform in the whole pre-chamber volume for each cycle with low levels of TKE reaching the spark plug gap. On the other hand, given that the holes of PC1c are faced directly toward each other, the crashing flow at the bottom of this design produces higher levels of turbulence that rise along the central part of the pre-chamber. Moreover, the snapshots of PC1c exhibit greater differences in both the local distribution of the TKE as it moves toward the spark plug, and the local intensity of the turbulence field. This is confirmed by the standard deviation column, where a much higher variation of the TKE between cycles is observed for PC1c compared to PC1.

Another important flow variable that must be analyzed is the velocity field. Therefore, Fig. 8 presents the same distribution of images

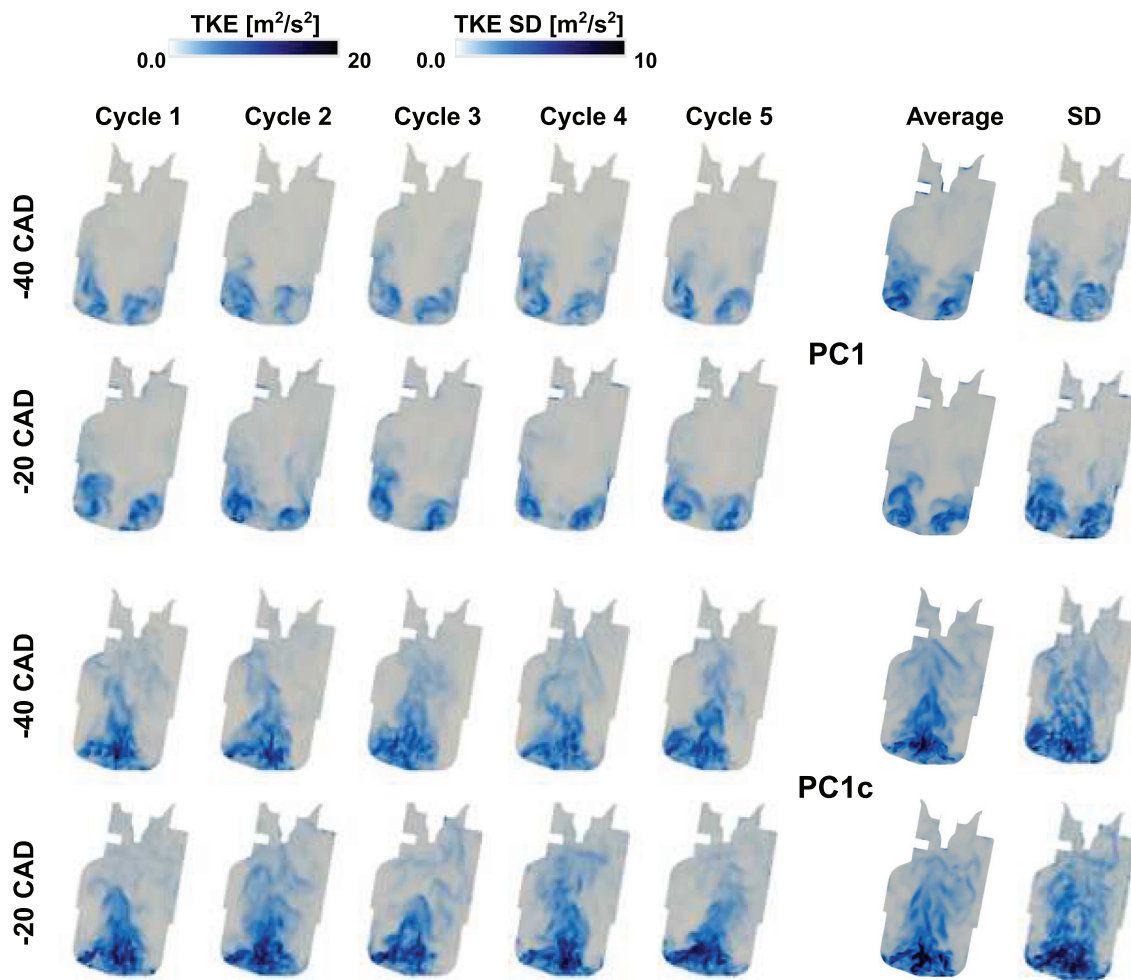


FIG. 7. Generation of turbulent kinetic energy inside the pre-chamber for the LES. Snapshots for PC1 are shown in the upper rows for five cycles at two crankangles, and in the bottom rows for PC1c. The time averaged and standard deviation of this parameter over all cycles is shown at the right-side of the figure for each pre-chamber at the corresponding crankangle.

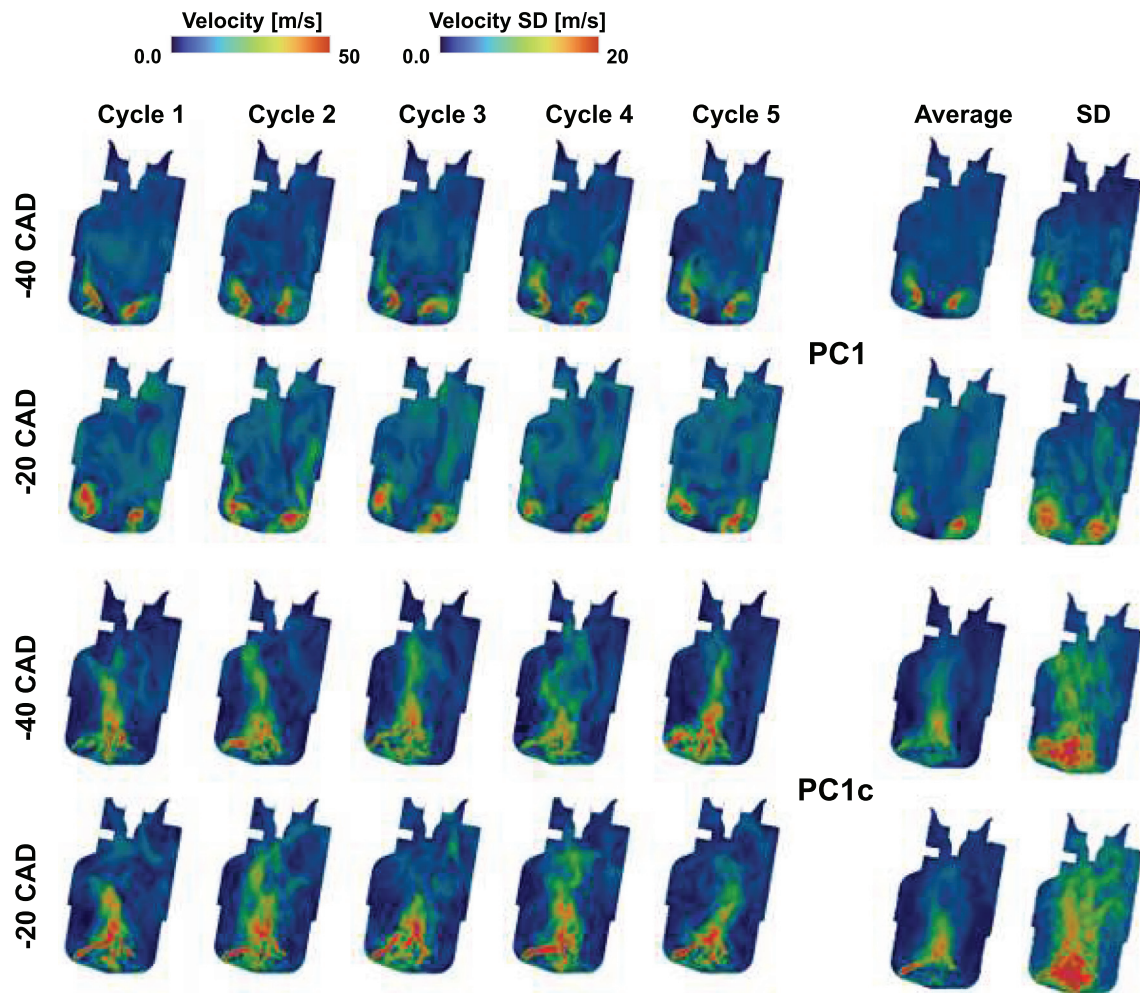


FIG. 8. Velocity field inside the pre-chamber for the LES. Snapshots for PC1 are shown in the upper rows for five cycles at two crankangles, and in the bottom rows for PC1c. The time averaged and standard deviation of this parameter over all cycles is shown at the right-side of the figure for each pre-chamber at the corresponding crankangle.

but for the velocity magnitude. It is interesting that despite showing the same pattern as the turbulence field, the local distribution of the velocity is much more uniform in the whole volume for PC1, without having such a high difference between the velocities at the bottom and at the top of the pre-chamber. On the other hand, PC1c shows a high stratification for this flow variable, where the velocities in the middle section of the pre-chamber are considerably higher than the near-wall regions. In addition, the consecutive snapshots also exhibit more differences compared to PC1, which is again highlighted by the standard deviation values. In this case, the levels of SD near the spark plug reach over 10 m/s for PC1c at -20 CAD, almost five times as high as the SD levels for PC1 in the same time frame.

Based on this initial assessment of the pre-chamber flow-field, PC1c begins to exhibit an unfavorable behavior in terms of cycle-to-cycle variation, as indicated by the higher standard deviation of the analyzed flow variables between cycles. However, the combustion simulations must be considered to complete the analysis.

B. Analyzing the combustion evolution in each pre-chamber design for different spark timings

Moving on to the reacting cases, Fig. 9 shows an overview of the combustion process for each design, with the spark triggered at -20 CAD. The evolution of the flame can be observed in the visualization images, where five snapshots are taken for two consecutive cycles. Regarding PC1, the initial flame kernel is very similar between the two cycles, and given that the swirling motion of the holes generates a uniform flow pattern, the morphology of the combustion process as it starts to progress throughout the pre-chamber is also alike for both cycles. In contrast, the initial snapshots of PC1c reveal a distinct ignition location. Consequently, the subsequent evolution of the flame exhibits greater disparities between the two cycles of this geometry. In addition, the particular flow pattern of PC1c bends the flame toward one side of the pre-chamber as it develops in this region.

In Fig. 10, the HRR profiles of the ten combustion cycles are plotted with the left column corresponding to PC1 and the right column

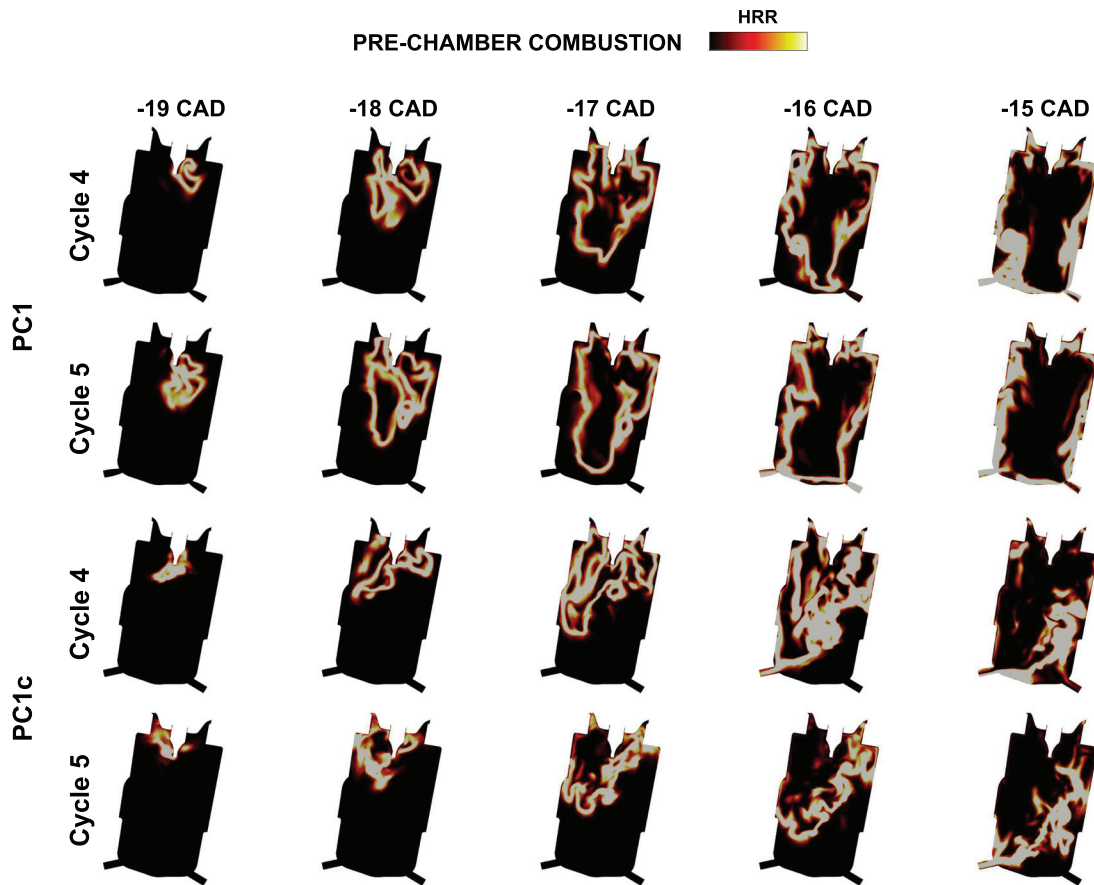


FIG. 9. Flame evolution inside PC1 and PC1c for two consecutive cycles.

to PC1c. From the top plots, it is clearly seen that the stabilized flow pattern helps PC1 to achieve faster burning rates than PC1c, and the combustion phasing for all cycles is kept within a short range. In contrast, the HRR profiles of PC1c exhibit more pronounced differences in terms of CA50 with an offset of approximately 2 CAD observed between the peak values of multiple cycles. This can be better observed in the bottom plots, where the average HRR of the ten cycles is presented for each pre-chamber, along with their corresponding standard deviations. Here, a higher SD is observed for PC1c due to greater variations in the combustion process between cycles.

Furthermore, Fig. 11 shows the cycle-averaged HRR of the five simulated spark timings, with their corresponding standard deviations. The black curves represent PC1 and the blue curves PC1c. For the reference case, with the ignition set to -20 CAD, the highest burn rates are achieved for both pre-chambers, showing also relatively low levels of dispersion. This matches the trends observed during the experimental campaign, given that the spark setting is the closest to the MBT conditions at low engine load and speed. However, when moving the ignition to either direction of this point, the SD values start to increase, especially for PC1c. At -5 CAD, for example, a 50% variation is observed for the peak HRR of the aforementioned pre-chamber.

At this point, one of the major issues found for the multi-cycle LES methodology was the difficulty to effectively quantify the CCV. Considering that the cyclic dispersion is evaluated for the indicated parameters of the engine (σ IMEP, COV IMEP), a suitable parameter for estimating the CCV was lacking from these simulations, given that only the pre-chamber combustion was modeled. For this purpose, the experimental spark timing sweep performed at low load/speed conditions (presented in Fig. 2) was contrasted with the results for the five simulated spark timings of PC1, in order to find a parameter that was able to reproduce the experimental trend.

In a first attempt, the maximum HRR value was considered. The bottom-right corner of Fig. 11 shows the comparison of the experimental COV IMEP and the covariance of the peak HRR (COV HRR_{max}) for the ignition sweep. It is clearly seen that the real behavior of the engine is not captured with this parameter. Fairly similar levels of COV HRR_{max} are obtained for each spark timing, showing the lowest value at -15 CAD, and failing to reproduce the flat tendency of the COV IMEP at early ignition times and the abrupt increase after -10 CAD. This can stem from the fact that the maximum HRR is not a parameter that directly relates to the ignition of the main chamber.

One of the phenomena that is usually overlooked when analyzing the pre-chamber system is the asymmetry with which the main

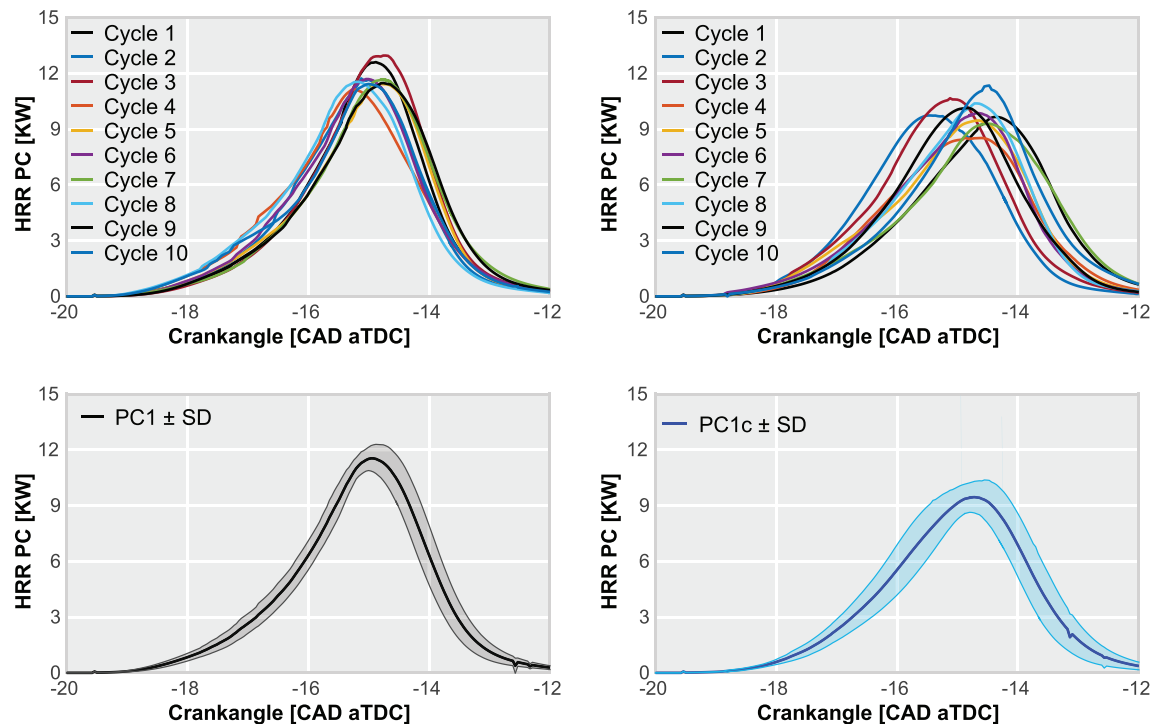


FIG. 10. Analysis of the HRR in each cycle of PC1 and PC1c with the spark triggered at -20 CAD.

chamber ignition can be generated. Considering that the flame can reach each hole at different time frames, as was observed in the flame evolution sequence of Fig. 9, some jets would be ejected before others, which could cause the flame to be quenched in certain cycles due to a premature pressurization of the main chamber. The asymmetric combustion pattern can lead to high cyclical dispersion since the flame evolution would change significantly in every engine cycle. Consequently, a characteristic parameter “ τ ” can be defined as the time it takes for the flame to reach each hole. Thus, this variable would represent an estimation of the main chamber combustion onset, as well as the morphology of the ignition source.

In light of the previous statement, monitor boxes were placed at the entrance of each hole for both pre-chamber designs, to determine the time at which the ECFM progress variable reaches a value of 0.55, which is the usual threshold used to define the flame front separating the burned gases (where the progress variable has a value of 1) and the unburned mixture (where the progress variable is null).⁶⁶

The results of this study are presented in Fig. 12 for the reference spark timing (upper row) and the most delayed spark timing (bottom row). These plots show the τ parameter in the vertical axis and the pre-chamber holes in the horizontal axis, labeled from 1 to 6. Each plotted line represents a combustion cycle; therefore, an ideal scenario would be characterized by overlapped horizontal lines, which indicates that the flame is reaching all the holes at the same time in every cycle. From here, the variations of the combustion process can be assessed in two directions (between holes and between cycles).

For PC1, the τ values are kept within a range of ± 1 CAD between cycles at the reference spark timing, showing a good combustion

stability. In addition, the behavior of τ in most cycles is relatively flat, with a variation of 0.5 CAD between holes, which also indicates a stable combustion evolution, leading to a uniform ignition of the main chamber. This can be further appreciated in the snapshots on the top plot of PC1, that are taken for a cut-plane perpendicular to the pre-chamber axis and just above the location of the holes. It can be seen that with a variation of only 1 CAD the flame is able to reach the pre-chamber bottom and sweep the whole circumference, promoting the ejection of reactive products throughout the six holes in a similar time frame. Moreover, for the delayed spark timing, the τ variations begin to increase (± 2 CAD between cycles); however, the behavior of the flame pattern between holes is still kept within a short range.

On the other hand, the behavior of τ for PC1c has higher deviations in both considered spark timings. First, the characteristic times for most cycles are higher than PC1, indicating that the flame takes longer to reach the pre-chamber bottom. This fact increases the energy losses due to non-reacting ejection of pre-chamber mixture,¹⁸ since the pressure builds up within the pre-chamber while the flame is still traveling through this region, and also increases the delay between the ignition signal and the onset of main chamber combustion, which has negative implications for the concept’s performance as was found in a previous study by Novella *et al.*³⁰ Second, the variations of τ between cycles are considerably higher, reaching a difference of up to 3 or even 4 CAD in both spark timings. Finally, the variance of τ between holes is also very high for some cycles, which can be seen in the upper snapshots of PC1c, where the flame is clearly reaching some holes sooner than others, making for an asymmetrical main chamber ignition.

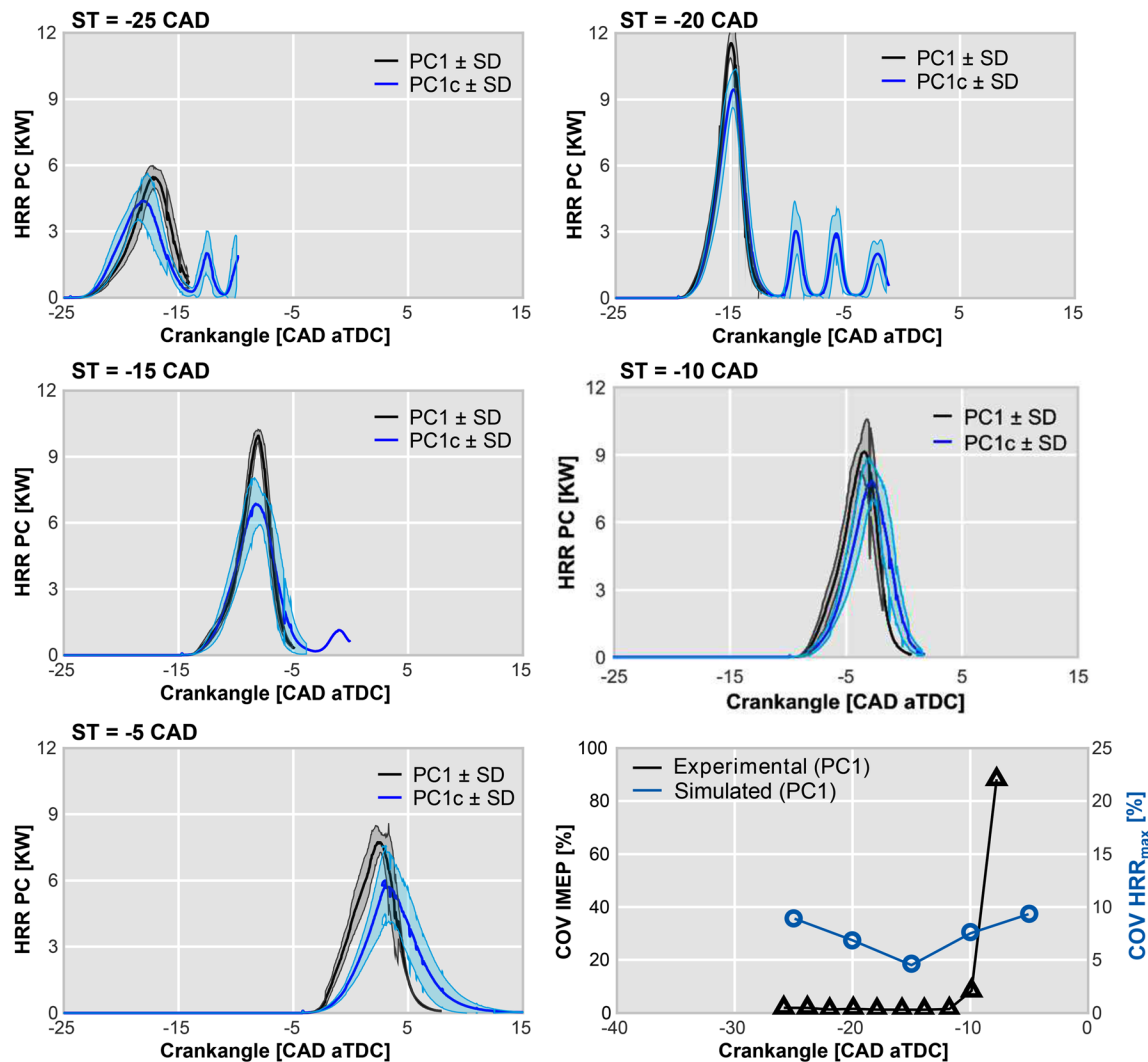


FIG. 11. HRR averaged over ten combustion cycles with the corresponding standard deviation for each pre-chamber at five different spark timings. The bottom-right corner shows the COV IMEP for the spark timing sweep performed in the real engine with PC1 at the simulated operating conditions, along with the COV of the peak HRR for each simulated spark timing.

This analysis suggests that PC1c is expected to have increased levels of CCV in a wide range of spark timings, compromising the performance of the engine, which correlates perfectly with the experimental trends found in Fig. 2. Moreover, to further prove the reliability of these results, Fig. 13 presents the covariance of the τ parameter compared to the experimental COV IMEP of PC1, highlighting that the experimental trend is very well matched with this new variable. Thus, these simulations are able to qualitatively predict the global tendencies of the concept and estimate the combustion stability threshold, proving the utility of the developed multi-cycle LES methodology for assessing the sources of CCV of different pre-chamber designs in SI engines.

Finally, this study has revealed an important conclusion related to the behavior of the passive pre-chamber concept in terms of cyclical dispersion. Although having higher levels of turbulence can (in

principle) help to accelerate the pre-chamber turbulent flame speeds, which is a feature that can essentially help to improve the performance of the concept, generating a stable flow pattern inside this region is predominant to maintain a fast and stable combustion process. This can be achieved by providing a tangential angle to the layout of the holes, enabling the generation of a swirling vortex that stabilizes the flow-field.

IV. SUMMARY AND CONCLUSIONS

This paper presents an innovative study about the impact of hole tangential angles in passive pre-chambers on the combustion stability of a light-duty SI engine. It began by presenting experimental results for two pre-chamber designs, one with a high tangential angle (PC1) and one with completely radial holes (PC1c). High levels of CCV were observed for PC1c at low engine load/speed conditions. Thereafter, a

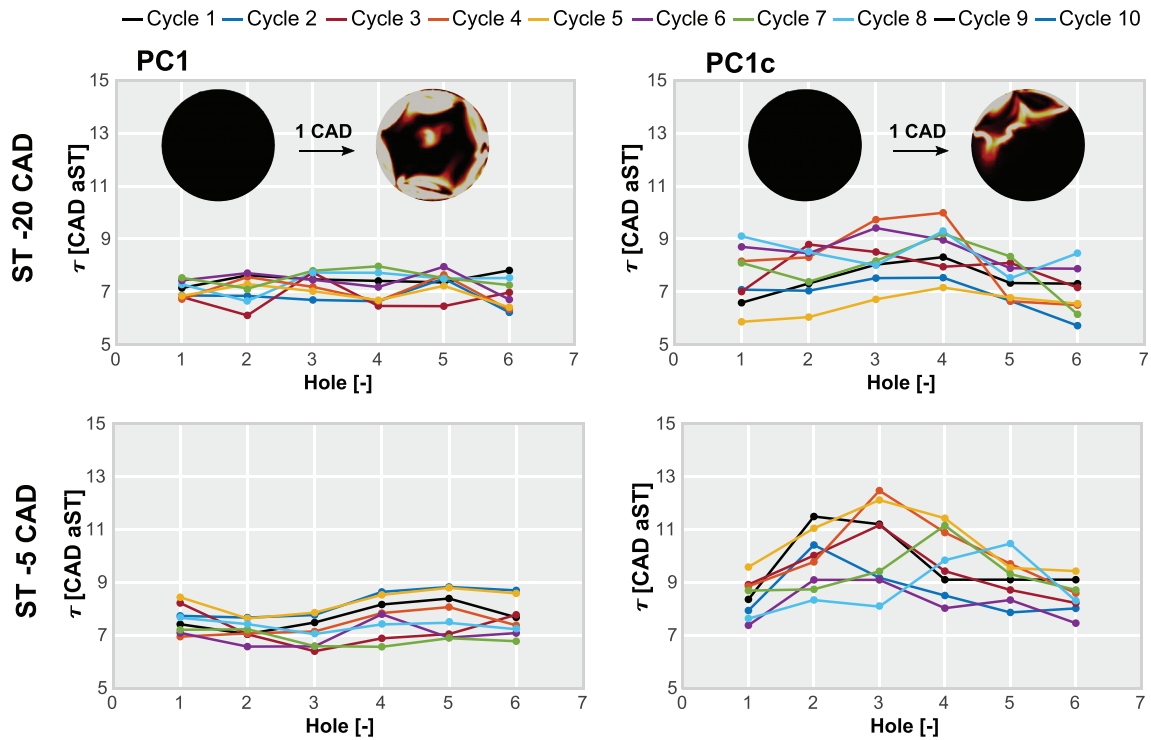


FIG. 12. τ values for each cycle at the reference and most delayed spark timings. The snapshots are shown for a cut-plane perpendicular to the pre-chamber axis just above the position of the holes.

CFD model, validated with the experimental data, was used to study both pre-chambers in depth. A modeling methodology was formulated for performing multi-cycle LES of the pre-chamber combustion, which allowed to execute a large number of simulations without consuming excessive computational resources. Although the approach did not account for thermodynamic and thermo-chemical stratification effects coming from the combustion process in the main chamber, meaningful correlations were found to support the validity of the developed methodology and offer insights into the behavior of the studied pre-chambers. The key findings of the investigation are as follows:

- A parameter was identified to evaluate the CCV levels associated with a specific pre-chamber design. The τ parameter, which measures the time it takes for the flame to reach each hole, relates the pre-chamber combustion to the main chamber ignition onset and morphology. High τ variations indicate asymmetric ignition, potentially causing cyclical dispersion. Furthermore, the covariance of τ matched the experimental COV IMEP trends for PC1, showing a reliable estimation of the combustion instability threshold of this pre-chamber.
- The analysis of PC1c revealed very high velocity and turbulent kinetic energy fluctuations in the whole pre-chamber volume, potentially contributing to poor CCV performance. The flow-field generated in this design proved to be undesirable for pre-chamber ignition systems, since it is challenging to stabilize combustion in these conditions. Particularly, designs with small holes (< 1 mm) will magnify this issue, given that the high TKE levels generated inside the pre-chamber could result in the blowing out of the initial flame kernel near the spark plug region, causing misfires.
- The undesirable flow-field of PC1c also causes the flame to evolve asymmetrically within this design, leading to high variations of τ between holes and between cycles for each simulated spark timing. This indicates an asymmetric ignition of the main chamber with some jets being ejected before others and different jets driving the combustion in every cycle. This pattern matches the experimental behavior of PC1c, where it is impossible to achieve a suitable combustion stability regardless of the employed spark timing.

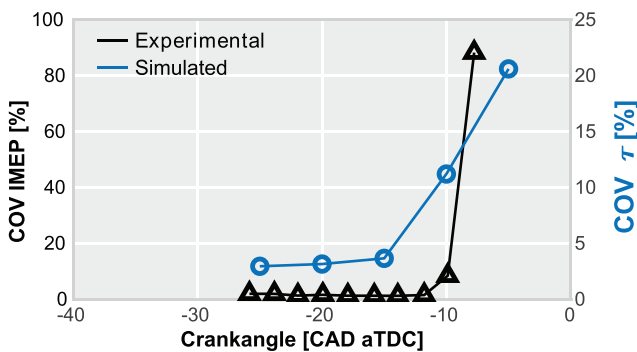


FIG. 13. Validation of the τ parameter with the experimental trend for the COV IMEP of PC1.

This research underscores the importance of a stable pre-chamber flow-field and emphasizes the significance of internal design and hole layout in enhancing the combustion stability. However, challenges remain, especially in idle or cold-start conditions, creating the need for further research into alternative design features, hole configurations, and internal geometries for practical implementation in passenger car engines. Future investigations could also extend to multi-cycle LES of the entire engine geometry to account for main chamber flow-field variations.

ACKNOWLEDGMENTS

The authors would like to express their gratitude to CONVERGENT SCIENCE, Inc. and Convergent Science GmbH for their kind support for the 0D, 1D, and CFD calculations with the CONVERGE software.

AUTHOR DECLARATIONS

Conflict of Interest

The authors have no conflicts to disclose.

Author Contributions

Ricardo Novella: Funding acquisition (equal); Investigation (equal); Methodology (equal); Project administration (equal). **Jose M. Pastor:** Investigation (equal); Methodology (equal); Writing – review & editing (equal). **Josep Gómez Soriano:** Conceptualization (equal); Formal analysis (equal); Investigation (equal); Methodology (equal); Writing – review & editing (equal). **Ibrahim Barbery:** Investigation (equal); Software (equal); Validation (equal); Visualization (equal); Writing – original draft (equal).

DATA AVAILABILITY

The data that support the findings of this study are available from the corresponding author upon reasonable request.

REFERENCES

- R. D. Reitz, H. Ogawa, R. Payri, T. Fansler, S. Kokjohn, Y. Moriyoshi, A. Agarwal, D. Arcoumanis, D. Assanis, C. Bae *et al.*, “IJER editorial: The future of the internal combustion engine,” *Int. J. Engine Res.* **21**, 3 (2020).
- S. Nalley and A. LaRose, *International Energy Outlook 2021 (IEO2021)* (US Department of Energy, 2021).
- European Environment Agency (EEA). *Transport Sector Contribution to Total GHG emissions (EEA-32)* (European Environment Agency, 2009).
- Z. Zhongming, L. Linong, Y. Xiaona, Z. Wangqiang, L. Wei *et al.*, *Transport: Increasing Oil Consumption and Greenhouse Gas Emissions Hamper EU Progress Towards Environment and Climate Objectives* (European Environment Agency, 2020).
- A. La Notte, S. Tonin, and G. Lucaroni, “Assessing direct and indirect emissions of greenhouse gases in road transportation, taking into account the role of uncertainty in the emissions inventory,” *Environ. Impact Assess. Rev.* **69**, 82–93 (2018).
- See https://www.acea.auto/files/20220720_PRPC-fuel_Q2-2022_FINAL.xlsx for E. A. O. A. M. (ACEA). “Data on Motor Vehicle Sales in the European Union in 2021 and 2022, Compiled by ACEA” (2022).
- J. R. Serrano, R. Novella, J. Gomez-Soriano, and P. J. Martinez-Hernandez, “Computational methodology for knocking combustion analysis in compression-ignited advanced concepts,” *Appl. Sci.* **8**(10), 1707 (2018).
- S. Cho, C. Song, N. Kim, S. Oh, D. Han, and K. Min, “Influence of the wall temperatures of the combustion chamber and intake ports on the charge temperature and knock characteristics in a spark-ignited engine,” *Appl. Therm. Eng.* **182**, 116000 (2021).
- S. Yu and M. Zheng, “Future gasoline engine ignition: A review on advanced concepts,” *Int. J. Engine Res.* **22**(6), 1743–1775 (2021).
- A. Jena, H. Singh, and A. K. Agarwal, “Effect of swirl ratio on charge convection, temperature stratification, and combustion in gasoline compression ignition engine,” *Phys. Fluids* **33**(8), 085113 (2021).
- R. Rajasegar, A. Srna, R. Novella, and I. Barbery, “Exploring the EGR dilution limits of a pre-chamber ignited heavy-duty natural gas engine operated at stoichiometric conditions-an optical study,” Technical Report No. 2023-01-0256 (SAE Technical Paper, 2023).
- L. Zhou, L. Zhong, P. Liu, Z. Feng, and H. Wei, “Experimental observation of the combustion modes based on a novel multistage pre-chamber turbulent jet ignition (TJI) system,” *Phys. Fluids* **35**(6), 066113 (2023).
- X. Liu, H. Aljabri, N. Panthi, A. S. AlRamadan, E. Cenker, A. T. Alshammari, G. Magnotti, and H. G. Im, “Computational study of hydrogen engine combustion strategies: Dual-fuel compression ignition with port-and direct-injection, pre-chamber combustion, and spark-ignition,” *Fuel* **350**, 128801 (2023).
- K. Bureshaid, R. Shimura, H. Zhao, D. Feng, and M. Bunce, “Investigation on knock resistance with turbulent jet ignition at different engine load in an optical engine,” Technical Report No. 2019-01-2151 (SAE Technical Paper, 2019).
- S. Heyne, M. Meier, B. Imbert, and D. Favrat, “Experimental investigation of prechamber autoignition in a natural gas engine for cogeneration,” *Fuel* **88**(3), 547–552 (2009).
- Y. Ye, Z. Yue, H. Wang, H. Liu, C. Wu, and M. Yao, “A mapping approach for efficient CFD simulation of low-speed large-bore marine engine with pre-chamber and dual-fuel operation,” *Energies* **14**(19), 6126 (2021).
- C. E. C. Alvarez, G. E. Couto, V. R. Roso, A. B. Thiriet, and R. M. Valle, “A review of prechamber ignition systems as lean combustion technology for SI engines,” *Appl. Therm. Eng.* **128**, 107–120 (2018).
- J. Benajes, R. Novella, J. Gomez-Soriano, I. Barbery, C. Libert, F. Rampanarivo, and M. Dabiri, “Computational assessment towards understanding the energy conversion and combustion process of lean mixtures in passive pre-chamber ignited engines,” *Appl. Therm. Eng.* **178**, 115501 (2020).
- S. Zhu, S. Akehurst, A. Lewis, and H. Yuan, “A review of the pre-chamber ignition system applied on future low-carbon spark ignition engines,” *Renewable Sustainable Energy Rev.* **154**, 111872 (2022).
- F. Di Sabatino, P. J. Martinez-Hernandez, R. Novella Rosa, and I. Ekoto, “Investigation on the effects of passive pre-chamber ignition system and geometry on engine knock intensity,” in *Internal Combustion Engine Division Fall Technical Conference* (American Society of Mechanical Engineers, 2022), Vol. 86540, p. V001T03A008.
- J. Cai, K. Sun, Y. Feng, M. Jia, Z. Lu, L. Shi, and T. Wang, “Turbulent jet ignition of ultra-lean methane/air mixture under engine-like condition,” *Phys. Fluids* **33**(11), 115121 (2021).
- P. Chinnathambi, B. Thelen, D. Cook, and E. Toulson, “Performance metrics for fueled and unfueled turbulent jet igniters in a rapid compression machine,” *Appl. Therm. Eng.* **182**, 115893 (2021).
- C. Müller, S. Pischinger, S. Tews, A. Müller, and K. Habermann, “Analysis of experimental results with an active pre-chamber ultra-lean burn SI engine,” *Int. J. Engine Res.* **22**(10), 3103–3127 (2021).
- F. Di Sabatino, P. J. Martinez-Hernandez, R. Novella Rosa, and I. Ekoto, “Investigation of the effects of passive pre-chamber nozzle pattern and ignition system on engine performance and emissions,” *Int. J. Engine Res.* **24**(6), 2592–2613 (2023).
- R. Payri, R. Novella, I. Barbery, and O. Bori-Fabra, “Numerical and experimental evaluation of the passive pre-chamber concept for future CNG SI engines,” *Appl. Therm. Eng.* **230**, 120754 (2023).
- A. Antolini, P. Sementa, C. Tornatore, F. Catapano, B. M. Vaglieco, J. M. Desantes, and J. J. López, “Effect of passive pre-chamber orifice diameter on the methane combustion process in an optically accessible SI engine,” *Fuel* **341**, 126990 (2023).
- A. Shah, P. Tunestal, and B. Johansson, “Effect of pre-chamber volume and nozzle diameter on pre-chamber ignition in heavy duty natural gas engines,” Technical Report No. 2015-01-0867 (SAE Technical Paper, 2015).
- J. Benajes, R. Novella, J. Gomez-Soriano, P. Martinez-Hernandez, C. Libert, and M. Dabiri, “Evaluation of the passive pre-chamber ignition concept for future

- high compression ratio turbocharged spark-ignition engines,” *Appl. Energy* **248**, 576–588 (2019).
- ²⁹J. Benajes, R. Novella, J. Gomez-Soriano, P. Martinez-Hernandez, C. Libert, and M. Dabiri, “Performance of the passive pre-chamber ignition concept in a spark-ignition engine for passenger car applications,” in *Proceedings of SIA Power Train & Electronics* (SIA Power Train & Electronics, Paris, 2019).
- ³⁰R. Novella, J. Gomez-Soriano, I. Barbary, and C. Libert, “Numerical analysis of the passive pre-chamber ignition concept for light duty applications,” *Appl. Therm. Eng.* **213**, 118610 (2022).
- ³¹M. Sens, E. Binder, P. Reinicke, M. Riess *et al.*, “Pre-chamber ignition and promising complementary technologies,” in *Proceedings of 27th Aachen Colloquium*, Aachen, 2018.
- ³²J. López, R. Novella, J. Gomez-Soriano, P. Martinez-Hernandez, F. Rampanarivo, C. Libert, and M. Dabiri, “Advantages of the unscavenged pre-chamber ignition system in turbocharged natural gas engines for automotive applications,” *Energy* **218**, 119466 (2021).
- ³³R. Novella, J. Gomez-Soriano, P. Martinez-Hernandez, C. Libert, and F. Rampanarivo, “Improving the performance of the passive pre-chamber ignition concept for spark-ignition engines fueled with natural gas,” *Fuel* **290**, 119971 (2021).
- ³⁴G. Maio, Z. Ding, K. Truffin, O. Colin, O. Benoit, and S. Jay, “ECFM-LES modeling with AMR for the ccv prediction and analysis in lean-burn engines,” *Sci. Technol. Energy Transition* **77**, 20 (2022).
- ³⁵O. Benoit, K. Truffin, S. Jay, J. van Oijen, Y. Drouvin, T. Kayashima, P. Adomeit, and C. Angelberger, “Development of a large-eddy simulation methodology for the analysis of cycle-to-cycle combustion variability of a lean burn engine,” *Flow, Turbul. Combust.* **108**, 559–598 (2022).
- ³⁶A. Broatch, R. Novella, J. García-Tiscar, J. Gómez-Soriano, and P. Pal, “Analysis of combustion acoustic phenomena in compression-ignition engines using large eddy simulation,” *Phys. Fluids* **32**(8), 085101 (2020).
- ³⁷Convergent Science Inc. *Converge 2.4 Theory Manual* (2018).
- ³⁸J. Benajes, R. Novella, J. Gomez-Soriano, I. Barbary, and C. Libert, “Advantages of hydrogen addition in a passive pre-chamber ignited SI engine for passenger car applications,” *Int. J. Energy Res.* **45**(9), 13219–13237 (2021).
- ³⁹V. Yakhot and S. A. Orszag, “Renormalization group analysis of turbulence. I. Basic theory,” *J. Sci. Comput.* **1**(1), 3–51 (1986).
- ⁴⁰R. Cant, “S. B. Pope, turbulent flows, Cambridge university press, Cambridge, UK,” *Combust. Flame* **125**, 1361–1362 (2001).
- ⁴¹A. Broatch, R. Novella, J. García-Tiscar, J. Gómez-Soriano, and P. Pal, “Investigation of the effects of turbulence modeling on the prediction of compression-ignition combustion unsteadiness,” *Int. J. Engine Res.* **23**(4), 541–559 (2022).
- ⁴²C. Chen, P. Pal, M. Ameen, D. Feng, and H. Wei, “Large-eddy simulation study on cycle-to-cycle variation of knocking combustion in a spark-ignition engine,” *Appl. Energy* **261**, 114447 (2020).
- ⁴³E. Pomraning and C. J. Rutland, “Dynamic one-equation nonviscosity large-eddy simulation model,” *AIAA J.* **40**(4), 689–701 (2002).
- ⁴⁴G. C. Krieger Filho, F. M. F. Silva, A. L. Pacifico, F. L. Sacomano Filho, C. B. Zabeu, F. B. Nigro, O. M. França, Jr., A. Penaranda, and P. T. Lacava, “Extended coherent flame model applied to an optical single-cylinder engine fueled with ethanol,” *Appl. Therm. Eng.* **236**, 121399 (2023).
- ⁴⁵G. Maio, A. Boberic, L. Giarracca, D. Aubagnac-Karkar, O. Colin, F. Duffour, K. Deppenkemper, L. Virnich, and S. Pischinger, “Experimental and numerical investigation of a direct injection spark ignition hydrogen engine for heavy-duty applications,” *Int. J. Hydrogen Energy* **47**(67), 29069–29084 (2022).
- ⁴⁶O. Colin, A. Benkenida, and C. Angelberger, “3D modeling of mixing, ignition and combustion phenomena in highly stratified gasoline engines,” *Oil Gas Sci. Technol.* **58**(1), 47–62 (2003).
- ⁴⁷O. Colin and A. Benkenida, “The 3-zones extended coherent flame model (ecfm3z) for computing premixed/diffusion combustion,” *Oil Gas Sci. Technol.* **59**(6), 593–609 (2004).
- ⁴⁸A. Jeevan Sai, R. Balamurugan, C. Servant, F. Ravet, and S. A. Kumar, “Applying ECFM combustion model to spark ignition engine, comparison with experimental data,” in *Advances in Fluid and Thermal Engineering: Select Proceedings of FLAME 2018* (Springer, 2019), pp. 729–741.
- ⁴⁹J. Duclos and O. Colin, “(2–25) arc and kernel tracking ignition model for 3D spark-ignition engine calculations ((SI-7) SI engine combustion 7-modeling),” in *The Proceedings of the International Symposium on Diagnostics and Modeling of Combustion in Internal Combustion Engines 01.204* (The Japan Society of Mechanical Engineers, 2001), p. 46.
- ⁵⁰O. Colin and K. Truffin, “A spark ignition model for large eddy simulation based on an FSD transport equation (ISSIM-LES),” *Proc. Combust. Inst.* **33**(2), 3097–3104 (2011).
- ⁵¹Y.-D. Liu, M. Jia, M.-Z. Xie, and B. Pang, “Enhancement on a skeletal kinetic model for primary reference fuel oxidation by using a semidecoupling methodology,” *Energy Fuels* **26**(12), 7069–7083 (2012).
- ⁵²H. Wang, M. Yao, and R. D. Reitz, “Development of a reduced primary reference fuel mechanism for internal combustion engine combustion simulations,” *Energy Fuels* **27**(12), 7843–7853 (2013).
- ⁵³L. Cai and H. Pitsch, “Optimized chemical mechanism for combustion of gasoline surrogate fuels,” *Combust. Flame* **162**(5), 1623–1637 (2015).
- ⁵⁴M. Mehl, W. J. Pitz, C. K. Westbrook, and H. J. Curran, “Kinetic modeling of gasoline surrogate components and mixtures under engine conditions,” *Proc. Combust. Inst.* **33**(1), 193–200 (2011).
- ⁵⁵J. Brakora and R. D. Reitz, “A comprehensive combustion model for biodiesel-fueled engine simulations,” Technical Report No. 2013-01-1099 (SAE Technical Paper, 2013).
- ⁵⁶K. Fieweger, R. Blumenthal, and G. Adomeit, “Self-ignition of SI engine model fuels: A shock tube investigation at high pressure,” *Combust. Flame* **109**(4), 599–619 (1997).
- ⁵⁷S. Jerzembeck, N. Peters, P. Pepiot-Desjardins, and H. Pitsch, “Laminar burning velocities at high pressure for primary reference fuels and gasoline: Experimental and numerical investigation,” *Combust. Flame* **156**(2), 292–301 (2009).
- ⁵⁸A. Torregrosa, P. Olmeda, B. Degrauwe, and M. Reyes, “A concise wall temperature model for DI diesel engines,” *Appl. Therm. Eng.* **26**(11–12), 1320–1327 (2006).
- ⁵⁹M. Lapuerta, O. Armas, and J. Hernández, “Diagnosis of di diesel combustion from in-cylinder pressure signal by estimation of mean thermodynamic properties of the gas,” *Appl. Therm. Eng.* **19**(5), 513–529 (1999).
- ⁶⁰F. Payri, S. Molina, J. Martín, and O. Armas, “Influence of measurement errors and estimated parameters on combustion diagnosis,” *Appl. Therm. Eng.* **26**(2), 226–236 (2006).
- ⁶¹P. Olmeda, J. Martín, R. Novella, and R. Carreño, “An adapted heat transfer model for engines with tumble motion,” *Appl. Energy* **158**, 190–202 (2015).
- ⁶²K. Truffin, C. Angelberger, S. Richard, and C. Pera, “Using large-eddy simulation and multivariate analysis to understand the sources of combustion cyclic variability in a spark-ignition engine,” *Combust. Flame* **162**(12), 4371–4390 (2015).
- ⁶³M. G. Masouleh, K. Keskinen, O. Kaario, H. Kahila, Y. M. Wright, and V. Vuorinen, “Flow and thermal field effects on cycle-to-cycle variation of combustion: Scale-resolving simulation in a spark ignited simplified engine configuration,” *Appl. Energy* **230**, 486–505 (2018).
- ⁶⁴M. G. Masouleh, K. Keskinen, O. Kaario, H. Kahila, S. Karimkashi, and V. Vuorinen, “Modeling cycle-to-cycle variations in spark ignited combustion engines by scale-resolving simulations for different engine speeds,” *Appl. Energy* **250**, 801–820 (2019).
- ⁶⁵C. Chen, M. M. Ameen, H. Wei, C. Iyer, F. Ting, B. Vanderwege, and S. Som, “LES analysis on cycle-to-cycle variation of combustion process in a DISI engine,” Technical Report No. 2019-01-0006 (SAE Technical Paper, 2019).
- ⁶⁶R. Novella, J. Pastor, J. Gomez-Soriano, I. Barbary, C. Libert, F. Rampanarivo, C. Panagiotis, and M. Dabiri, “Experimental and numerical analysis of passive pre-chamber ignition with EGR and air dilution for future generation passenger car engines,” Technical Report No. 2020-01-0238 (SAE Technical Paper, 2020).